Effect of soil roughness on the inversion of off-ground monostatic GPR signal for noninvasive quantification of soil properties

Sébastien Lambot, 1,2 Michaël Antoine, Marnik Vanclooster, and Evert C. Slob1

Received 7 July 2005; revised 14 November 2005; accepted 30 November 2005; published 7 March 2006.

We report on a laboratory experiment that investigates the effect of soil surface roughness on the identification of the soil electromagnetic properties from full-wave inversion of ground-penetrating radar (GPR) data in the frequency domain. The GPR system consists of an ultrawide band stepped-frequency continuous-wave radar combined with an off-ground monostatic horn antenna. Radar measurements were performed above a rectangular container filled with a loose sandy soil subject to seven water contents and four random surface roughnesses, including a smooth surface as reference. Compared to previous studies, we have reduced the modeling error of the GPR signal for the smooth surface case thanks to improved antenna transfer functions by solving an overdetermined system of equations based on six model configurations instead of only three. Then, the continuously increasing effect of surface roughness on the radar signal with respect to frequency is clearly observed. In close accordance with Rayleigh's criterion, both the radar signal and the inversely estimated parameters are not significantly affected if the surface protuberances are smaller than one eighth of a wavelength. In addition, when this criterion is not respected, errors are made in the estimated parameters, but the inverse solution remains stable. This demonstrates the promising perspectives for application of GPR for noninvasive water content estimation in agricultural and environmental field applications.

Citation: Lambot, S., M. Antoine, M. Vanclooster, and E. C. Slob (2006), Effect of soil roughness on the inversion of off-ground monostatic GPR signal for noninvasive quantification of soil properties, *Water Resour. Res.*, 42, W03403, doi:10.1029/2005WR004416.

1. Introduction

[2] Knowledge of the dynamics of water and solute or pollutant transfer in soil-plant-atmosphere or biogeosystems is essential in agricultural, hydrological, and environmental research and engineering as it controls, at different scales, key hydrological processes, plant growth, contamination of surface and subsurface water, sustainability of natural ecosystems and biodiversity, and climate change. Specific features of biogeosystems are their inherent spatial and temporal variability, the inaccessibility of the subsurface, which hinders the observation of relevant processes, and the interconnectivity of different subsystems, which requires a holistic approach. Therefore there is a strong need for the development and integration of novel techniques, which allow noninvasive monitoring of both surface and subsurface processes at spatial scales relevant for the understanding and management of biogeosystems.

[3] Sensitivity of radar backscatter to soil water content has led to a considerable interest in exploiting radar data [4] At all radar characterization scales, soil surface roughness conditions have been a major difficulty in the development of soil property retrieval algorithms. Soil surface roughness is considered as a major source of clutter in various subsurface sensing applications [El-Shenawee and Miller, 2004], e.g., as in soil surface water content mapping or landmine detection. In particular, surface roughness may cause considerable distortion to electromagnetic signals and needs to be taken into account in signal processing [e.g., Chanzy et al., 1996]. When the reflection surface is smooth, most of the recorded energy comes from the specular

Copyright 2006 by the American Geophysical Union. 0043-1397/06/2005WR004416

W03403 1 of 10

collected by spaceborne satellites, airborne and groundbased radar systems for the retrieval of hydrologic information at different scales. For example, catchment-scale (10–1000 km²) hydrologic characterization is possible by means of synthetic aperture radars (SAR) which yield the appropriate spatial resolution (10-100 m) [e.g., Mancini et al., 1999]. Development of new techniques is still needed to bridge the gap between airborne/spaceborne remote sensing scales and the ground truth measurement scale (1-10 cm). In this regard, ground-penetrating radar (GPR) is increasingly used as a near-surface remote sensing tool. Many studies have investigated the potential of GPR for estimating soil water content [Du and Rummel, 1994; Chanzy et al., 1996; van Overmeeren et al., 1997; Weiler et al., 1998; Huisman et al., 2001]. Excellent reviews are given by Davis and Annan [2002] and Huisman et al. [2003].

¹Department of Geotechnology, Delft University of Technology, Delft, Netherlands.

²Now at Agrosphere (ICG-IV) Institute of Chemistry and Dynamics of the Geosphere, Forschungszentrum Jülich GmbH, Jülich, Germany.

³Department of Environmental Sciences and Land Use Planning, Université catholique de Louvain, Louvain-la-Neuve, Belgium.

reflection (coherent component). However, when the surface is rough, diffuse reflection (incoherent component) can occur; this situation is better known as scattering.

- [5] Modeling electromagnetic scattering from rough surfaces has been the object of theoretical and experimental studies for many years. Various available analyses and numerical simulations have shown the considerable complexity of rough surface scattering [Beckmann and Spizzichino, 1987; Michalski and Zheng, 1990; Chen and Bai, 1990; Hastings et al., 1995]. Recent studies on scattering from rough surfaces have been carried out in the frequency and time domains [O'Neill et al., 1996; Zhang et al., 1997; Dogaru and Carin, 2001; Yarovoy et al., 2004]. In this respect, a general approach for estimating and subsequently disentangling the relative influences of soil moisture and roughness on the backscattering coefficient is to make use of physically based scattering models [Fung et al., 1992; Chen and Fung, 1995]. A review on numerical methods in the study of electromagnetic scattering from random rough surfaces is given by Warnick and Chew [2001].
- [6] These previous approaches concentrated on airborne and spaceborne remote sensing, which focus on the surface reflection coefficient. For GPR, the roughness issue has already been investigated for some imaging applications [Sai and Ligthart, 2004; Yarovoy et al., 2004] or antenna radiation analysis [Lampe and Holliger, 2003], but still remains largely unexplored for the retrieval of the soil electromagnetic properties. Usually, only the soil dielectric permittivity is determined from GPR data and is derived from the wave propagation time between the emitting and receiving antennas. Recently, Lambot et al. [2004c, 2004d] proposed a new promising approach for identifying the soil hydrogeophysical properties using GPR. Relying on an electromagnetic model describing remarkably well the radar-antenna-subsurface system, the method is based on fullwave inversion of the GPR signal in the frequency domain for an off-ground monostatic configuration. The approach has been validated in laboratory conditions for identifying both the dielectric permittivity and electric conductivity of a two-layered sandy soil subject to a range of water contents [Lambot et al., 2004d], to identify a continuous water content profile in controlled outdoor conditions using hydrostatic concepts [Lambot et al., 2004b], to monitor the dynamics of water in a sand column and subsequently derive the soil hydraulic properties using hydrodynamic inverse modeling [Lambot et al., 2004a], to investigate the frequency dependence of the soil dielectric permittivity and electric conductivity of a sandy soil for different water contents [Lambot et al., 2005a], and to specifically map the surface water content by focusing the full-wave inversion on the surface wave reflection [Lambot et al., 2005b]. The approach presents unique advantages compared to existing and commonly used GPR characterization methods, which are based essentially on the determination of the wave propagation time [Huisman et al., 2003]. The main advantages are as follows: (1) it permits control of an ultrawide frequency band and therefore to get retrieval of more information from the ground on soil properties. (2) The system uses only one antenna off the ground, which reduces the cost of the system and improves mobility. (3) Since handheld vector network analyzers are nowadays readily available tools, they can be used to emulate GPR at low cost

and with a high portability. (4) The adequacy of the antenna model permits the use of full-wave electromagnetic inverse modeling techniques to analyze the signal and therefore to consider all the information contained in the signal, including the propagation time and amplitude. (5) It permits identification of the electric conductivity and its frequency dependence, in contrast to any other existing GPR approaches.

[7] This paper extends previous work by investigating quantitatively the sensitivity of the radar signal and inversely estimated soil electromagnetic parameters to soil surface roughness. It constitutes therefore the next logical step toward the application of the proposed GPR approach in practical field situations as encountered in agriculture or environmental engineering. To the best of our knowledge, this is the first time that such a quantitative analysis of the GPR signal is used to estimate the soil electromagnetic properties via full-wave inverse modeling. For this purpose, radar measurements were performed in the laboratory for different surface roughness and water content conditions. In addition, we provide in this paper a method to improve the characterization of the antenna properties that reduces the mismatch between the radar measurements and the electromagnetic forward model.

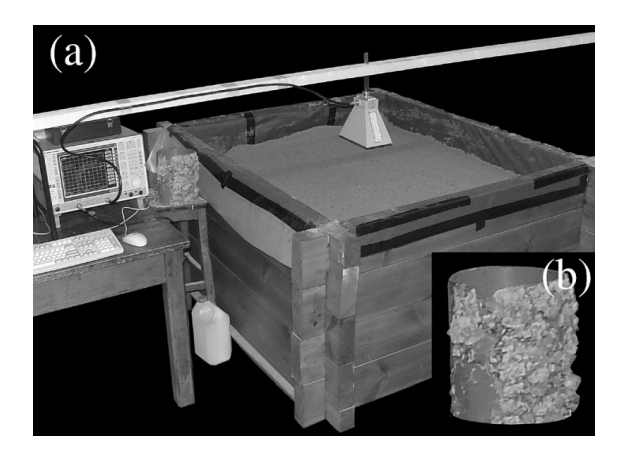
2. Materials and Methods

2.1. Laboratory Experimental Setup

- [8] Laboratory experiments were conducted at the Royal Military Academy of Brussels (Belgium). Figure 1 represents the experimental setup. Radar measurements were performed above a rectangular container (1.45 × 1.30 m² area) made of wood and filled with a one-layered sandy soil (0.09 m thick). Below the sand layer, a horizontal metal sheet was installed to control the bottom boundary condition in the electromagnetic model. Indeed, materials underneath this metal sheet have no influence on the measured back-scattered signal. The sand was subject to seven water contents from dry to wet conditions and four surface roughness levels, including a smooth surface, resulting in 28 independent configurations.
- [9] Starting from dry conditions, the different water content levels were imposed successively by adding water on the sand, and by mixing manually sufficiently long to obtain a homogeneous distribution of the water within the whole sand layer. Water content at the GPR scale was indirectly derived from the GPR signal following the approach presented in *Lambot et al.* [2004d], namely, from full-wave inversion of off-ground monostatic GPR signal in the frequency domain. Since the same sandy soil was used, we related the GPR derived dielectric permittivity to the volumetric water content using the same relationship derived for a smooth surface, namely,

$$\theta = 2.30 \times 10^{-4} \varepsilon_r^3 - 6.28 \times 10^{-3} \varepsilon_r^2 + 7.50 \times 10^{-2} \varepsilon_r - 1.51 \times 10^{-1}$$
(1)

where θ is the volumetric water content and ε_r is the relative dielectric permittivity. After measuring the water content of the sandy soil with a smooth surface the surface was perturbed. At each water content, we pressed stamps with



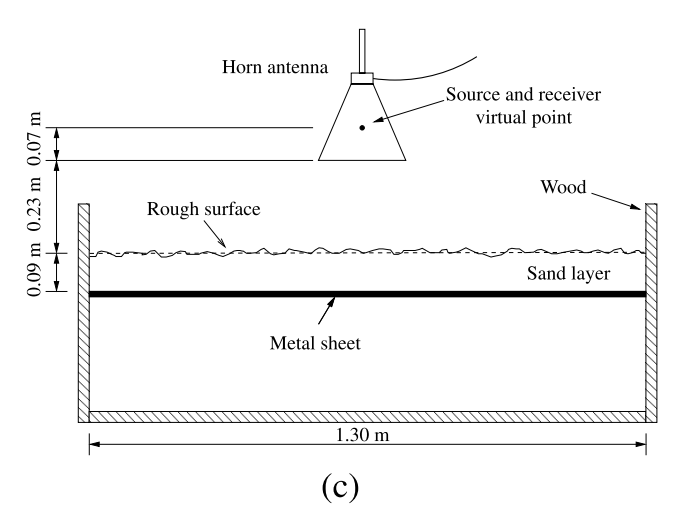


Figure 1. (a, b) Photographs and (c) scheme of the laboratory experimental setup, including the sand box made of wood, the VNA and off-ground horn antenna, and the rough sand layer with a metal sheet at the bottom to control the boundary condition in the electromagnetic model. Shown in Figure 1b, the cylindrical stamp with pebbles randomly glued to the surface was used to produce random roughness.

different surface roughnesses into the sand. For this purpose, a cylinder with stones randomly glued onto the surface was squeezed over the smooth sand surface, applying sufficient pressure to produce the desired roughness topography.

2.2. Radar Measurements

[10] As described by *Lambot et al.* [2004c, 2004d], we used an ultrawide band stepped-frequency continuous-wave radar combined with an off-ground monostatic horn antenna. The radar system was set up using a vector network analyzer (VNA, ZVRE, Rohde&Schwarz) with an excellent dynamic range (>130 dB). The antenna system consisted of a linear polarized double-ridged broadband horn (BBHA 9120 D, Schwarzbeck Mess-Elektronik). Antenna dimensions are 22 cm length and 14 × 24 cm² aperture area. The nominal frequency range is 1–18 GHz and isotropic gain ranges from 6–18 dBi. The relatively small 3–dB beam width of the antenna (27° in the E plane and 22° in the H plane at 2 GHz) makes it suitable for using off ground. Measure-

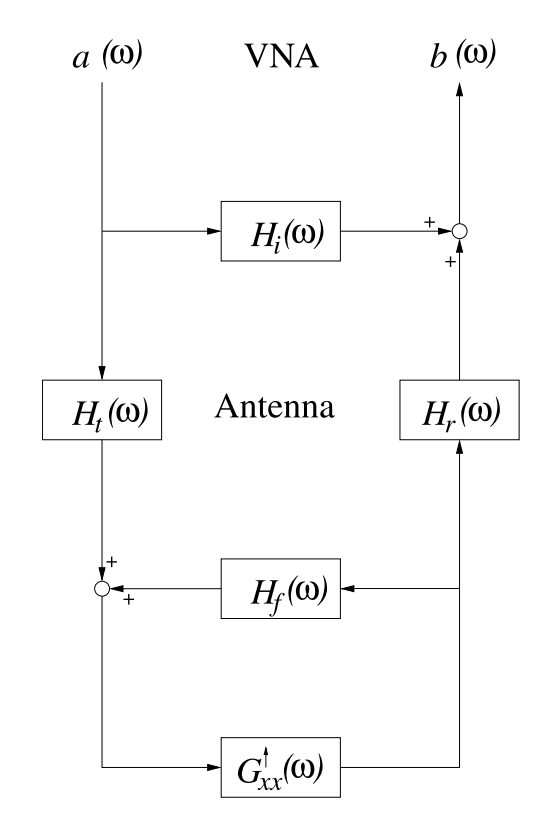
ments were performed with the antenna aperture situated at an average height of 23 cm above the soil surface.

[11] The antenna was connected to the reflection port of the VNA via a high quality N-type 50 Ohm impedance coaxial cable of 2.5 m length (Sucoflex 104PEA, Huber+Suhner). We calibrated the VNA at the connection between the antenna feed point and the cable. The frequency-dependent complex ratio $S_{11}(\omega)$ between the received and emitted wave was measured sequentially at 501 evenly stepped operating frequencies over the range 1–3 GHz using a 4 MHz frequency step, ω being the angular frequency.

2.3. Modeling of the Radar Signal

2.3.1. Radar Equation

[12] The radar-antenna-subsurface system is modeled using the block diagram represented in Figure 2 [Lambot et al., 2004d]. This model of complex scalar and linear transfer functions assumes that the shape of the electromagnetic field received by the antenna is independent of the target, i.e., only the phase and amplitude of the field are function of the target. This has been proven [Lambot et al., 2004d, 2005a] to be a valid assumption when the antenna is located not too close above a horizontally multilayered



Multilayered medium

Figure 2. Block diagram representing the VNA antenna multilayered medium system modeled as linear systems in series and parallel, where b and a are the received and emitted waves at the VNA reference plane, respectively, H_i is the return loss, H_t and H_r are the transmitting and receiving transfer functions, respectively, H_f is the feedback loss, and G_{xx}^{\dagger} is the transfer Green's function of the air-subsurface system.

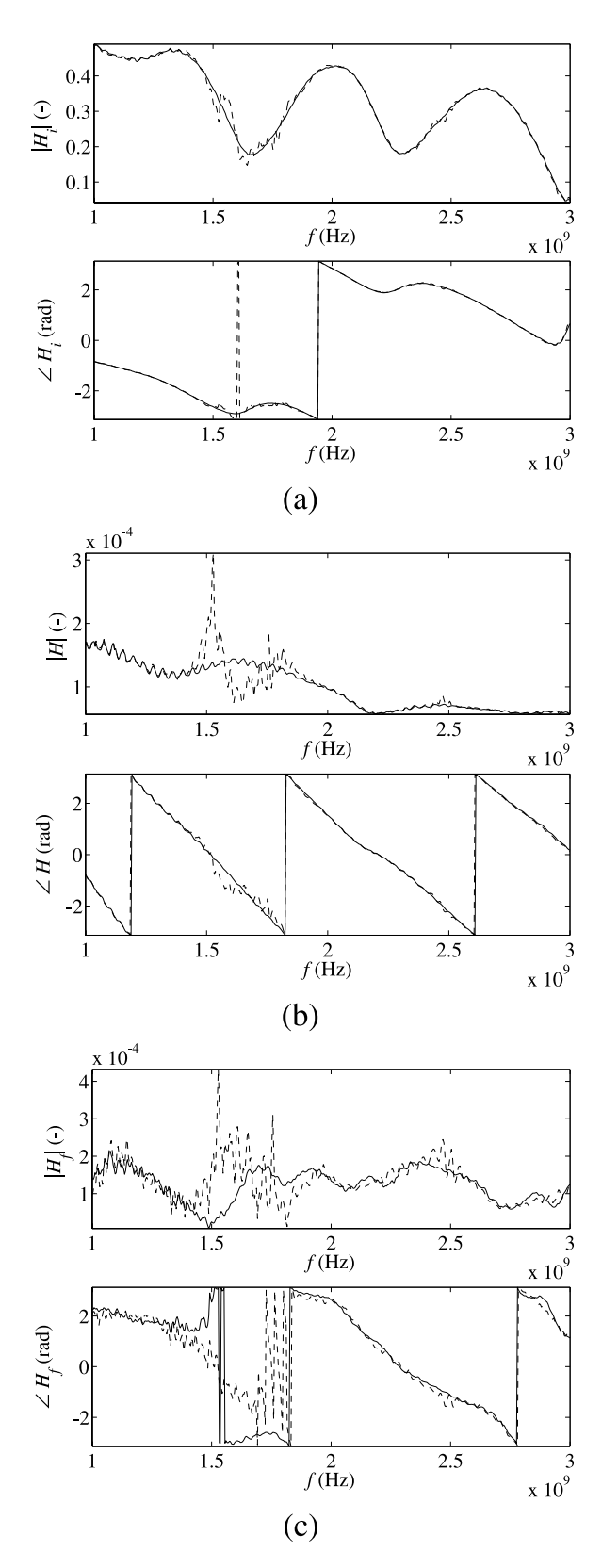


Figure 3. Antenna transfer functions for n = 3 model configurations (three equations as (2) to solve for the three unknowns H_i , H, and H_f , dashed lines) and n = 6 (overdetermined system of equations, solid lines): (a) return loss H_i , (b) transmitting-receiving transfer function H, and (c) feedback loss H_f .

medium representing the subsurface. The corresponding transfer function, expressed in the frequency domain, is given by

$$S_{11}(\omega) = \frac{b(\omega)}{a(\omega)} = H_i(\omega) + \frac{H(\omega)G_{xx}^{\uparrow}(\omega)}{1 - H_f(\omega)G_{xx}^{\uparrow}(\omega)}$$
(2)

where $b(\omega)$ and $a(\omega)$ are, respectively, the received and emitted waves at the VNA reference plane, $H_i(\omega)$ is the return loss, $H(\omega) = H_i(\omega)H_r(\omega)$ is the transmitting-receiving transfer function, $H_j(\omega)$ is the feedback loss, and $G_{xx}^{\uparrow}(\omega)$ is the transfer function of the air-subsurface system modeled as a three-dimensional multilayered medium.

2.3.2. Improved Determination of the Antenna Transfer Functions

[13] The characteristic transfer functions $H_i(\omega)$, $H(\omega)$ and $H_f(\omega)$ can be determined by solving the system of equations (2) for three different model configurations (denoted k). We use well defined model configurations with the antenna situated at different heights above a metal sheet playing the role of an infinite perfect electric conductor. The Green functions $G^{\uparrow}_{xx,k}(\omega)$ can therefore be computed, while the functions $S_{11,k}(\omega)$ can be readily measured. It is worth noting that the return loss transfer function $H_i(\omega)$ can also be measured directly by performing measurements in free space conditions, i.e., for which $G^{\uparrow}_{xx}(\omega) = 0$. In practical situations, we use measurements with the antenna directed toward the sky.

[14] In previous studies, we usually considered n = 3configurations. However, for some frequencies the solution of the system of equations may be numerically not stable, depending on the different considered distances between the antenna and the metal sheet. This is due to correlation between the equations of system (2) inherently present when spanning a wide frequency range resulting in significant errors in the determination of the antenna transfer functions. To overcome this problem, we recommend in this paper to have n > 3, resulting in an overdetermined system of equations. As an example, Figure 3 represents the antenna transfer functions determined using n = 3 (dashed line) and n = 6 (solid line). In this example, the different heights of the antenna aperture above the metal sheet were, respectively, 0.307, 0.354, 0.392, 0.432, 0.490, and 0.645 m. For n = 3, with heights settings at 0.307, 0.392, and 0.490 m, inaccurate values for the transfer functions are obtained for discrete frequencies.

[15] To solve the overdetermined system of equations, equation (2) can be linearized as follows:

$$S_{11,k} = H_i + S_{11,k} G_{yyk}^{\uparrow} H_f + G_{yyk}^{\uparrow} (H - H_i H_f)$$
 (3)

The resulting linear system of equations can be written in matrix form as

$$\mathbf{b} = \mathbf{A}\mathbf{x} \tag{4}$$

where

$$\mathbf{b} = \begin{bmatrix} S_{11,1} \\ \vdots \\ S_{11,k} \\ \vdots \\ S_{11,n} \end{bmatrix}$$
 (5)

$$\mathbf{A} = \begin{bmatrix} 1 & S_{11,1}G_{xx,1}^{\uparrow} & G_{xx,1}^{\uparrow} \\ \vdots & \vdots & \vdots \\ 1 & S_{11,k}G_{xx,k}^{\uparrow} & G_{xx,k}^{\uparrow} \\ \vdots & \vdots & \vdots \\ 1 & S_{11,n}G_{xx,n}^{\uparrow} & G_{xx,n}^{\uparrow} \end{bmatrix}$$

$$\mathbf{x} = \begin{bmatrix} H_i \\ H_f \\ H - H_i H_f \end{bmatrix}$$

$$(6)$$

Then, the vector of unknowns is in the least squares sense computed as

$$\mathbf{x} = \left(\mathbf{A}^{\mathsf{H}}\mathbf{A}\right)^{-1}\mathbf{A}^{\mathsf{H}}\mathbf{b} \tag{8}$$

where symbol $\underline{\underline{H}}$ denotes the Hermitian or conjugate transpose $(\underline{A}^H \equiv \overline{\underline{A}}^T)$.

2.3.3. Soil Electromagnetic Properties

[16] The constitutive parameters governing electromagnetic wave propagation are the dielectric permittivity ε (Fm^{-1}) , electric conductivity σ (Sm^{-1}) , and magnetic permeability μ (Hm⁻¹). We assume μ equal to the permeability of free space, namely, $\mu_0 = 4\pi \times 10^{-7} \text{ Hm}^{-1}$, which is valid for non magnetic soil materials as prevalent in most subsurface environments. The relative dielectric permittivity is defined as $\varepsilon_r = \varepsilon/\varepsilon_0$, where $\varepsilon_0 = 1/(\mu_0 c_0^2)$ is the permittivity of free space with $c_0 = 299792458 \text{ ms}^{-1}$ being the speed of light in vacuum. Because of relaxation mechanisms and Maxwell-Wagner effects, soil materials can exhibit a frequency dependence in the GPR frequency range [Hipp, 1974; Hallikainen et al., 1985; Heimovaara et al., 1996; West et al., 2003]. In accordance with the results of Lambot et al. [2005a] for the same sandy soil, we assume in this paper a frequency independent dielectric permittivity and a linearly frequency dependent electric conductivity described by

$$\sigma(f) = \sigma_{1\text{GHz}} + a(f - 10^9) \tag{9}$$

where $\sigma_{1 \text{GHz}}$ is the reference electric conductivity at 1 GHz, and a is the linear variation rate of $\sigma(f)$. It is worth noting here that σ represents an effective or apparent electric conductivity, as it includes dielectric losses which cannot be characterized apart.

2.3.4. Air-Subsurface Green's Function

[17] The air-subsurface system is modeled as a three-dimensional multilayered medium consisting of N horizontal layers separated by N-1 interfaces. The medium of the nth layer is homogeneous and characterized by ε_n , σ_n , and thickness h_n . Given the monostatic antenna configuration and assuming the subsurface as a horizontally multilayered medium to be located in the far-field region of the antenna, the shape of the antenna radiation pattern has little influence on the measured radar signal and the antenna can be approximated by a point source and receiver located in the upper half-space [Balanis, 1997; Lambot et al., 2004d]. The emitting part of the horn antenna is approximated by an infinitesimal horizontal x-directed electric dipole (second subscript x in G_{xx}^{\uparrow}), whereas the receiving part of the antenna is emulated by recording the horizontal x-directed compo-

nent (first subscript x in G_{xx}^{\uparrow}) of the backscattered electric field (up arrow in G_{xx}^{\uparrow}).

[18] The consideration of a three-dimensional model is essential to take into account spherical divergence (geometrical spreading) in wave propagation and the existence of TE mode (transverse electric) and TM mode (transverse magnetic) waves within the first Fresnel zone that contribute to the recorded signal, each with a different reflection coefficient at interfaces. The Green's function, i.e., the solution of Maxwell's equations, for electromagnetic waves propagating in multilayered media is well known [*Tai*, 1994; *Michalski and Mosig*, 1997; *Peterson et al.*, 1998]. We adopted the approach as described by *Slob and Fokkema* [2002] and *Lambot et al.* [2004d].

2.4. Model Inversion

[19] We formulate the inverse problem in the least squares sense and the objective function is accordingly defined as follows:

$$\phi(\mathbf{b}) = \left| \mathbf{G}_{\mathbf{x}\mathbf{x}}^{\uparrow \star} - \mathbf{G}_{\mathbf{x}\mathbf{x}}^{\uparrow} \right|^{T} s_{err}^{-2} \left| \mathbf{G}_{\mathbf{x}\mathbf{x}}^{\uparrow \star} - \mathbf{G}_{\mathbf{x}\mathbf{x}}^{\uparrow} \right|, \tag{10}$$

where $\mathbf{G}_{\mathbf{xx}}^{\uparrow *} = G_{\mathbf{xx}}^{\uparrow *}(\omega)$ and $\mathbf{G}_{\mathbf{xx}}^{\uparrow} = G_{\mathbf{xx}}^{\uparrow}(\omega, \mathbf{b})$ are the vectors containing, respectively, the observed and simulated airsubsurface transfer or Green's functions, \mathbf{b} is the parameter vector to be estimated and defined as $\mathbf{b} = [\varepsilon_r, \sigma_{1\text{GHz}}, a, h]$, and s_{err}^2 is the measurement error variance. Parameters ε_r , $\sigma_{1\text{GHz}}$, and a are the sand electromagnetic properties and h is the distance between the antenna source and receiver point, i.e., antenna phase center, and the soil surface. The thickness of the sand layer is then derived knowing the fixed distance between the antenna and the metal sheet. These vectors are arranged versus angular frequency. Since these response functions are complex functions, the difference between observed and modeled data is expressed by the amplitude of the errors in the complex plane.

[20] Objective function (10) has inherently a nonlinear topography, containing several local minima, and is minimized by means of the global multilevel coordinate search algorithm [Huyer and Neumaier, 1999] combined sequentially with the classical Nelder-Mead simplex algorithm [Lagarias et al., 1998]. We refer to Lambot et al. [2002, 2004c] for additional details about this optimization procedure. Inversions took place in a large parameter space (2.5 < $\varepsilon_r < 15$; $1 \times 10^{-3} < \sigma_{1\rm GHz} < 1 \times 10^{-1} \, {\rm Sm}^{-1}$; $1 \times 10^{-12} < a < 1 \times 10^{-10} \, {\rm Ssm}^{-1}$; $0.24 < h < 0.34 \, {\rm m}$) which contained all the solutions corresponding to the 28 considered scenarios (7 water contents \times 4 roughnesses).

2.5. Surface Roughness Characterization

[21] A rough surface can be described mathematically as $h = h(\mathbf{r})$, where h denotes the height of the rough surface with respect to a smooth reference surface, and \mathbf{r} is the position vector of points on the reference surface. For a random rough surface, the height fluctuation is a random parameter with respect to the position and is characterized by a stochastic process. In theoretical models of rough surface scattering, it is often assumed that the surface is stationary with a random Gaussian height distribution [Dierking, 1999; Davidson et al., 2000]. In this case, the mean and variance of the elevation, and the autocorrelation function (which is related to the horizontal length scale of

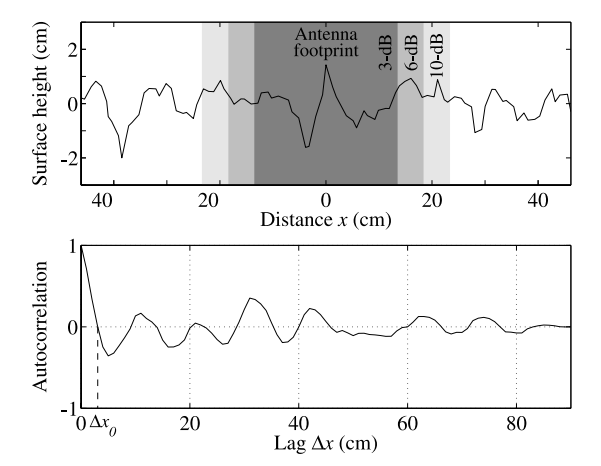


Figure 4. Soil surface topography compared to the antenna footprint in the E plane and related normalized autocorrelation function for roughness R_4 (average standard deviation s=0.72 cm, average maximal amplitude of the protuberances $h_{\rm max}=3.8$ cm) and water content $\theta=0.12$. For all roughness scenarios considered in this study, except for the smooth surface cases, the correlation length Δx_0 varies from about 2 to 5 cm.

height variation) provide a complete description of the statistical surface properties.

[22] For applications in radar data analysis, topography needs to be sampled with a horizontal resolution $\Delta x \leq$

 0.1λ , where λ is the radar wavelength [Dierking, 1999]. This is only valid for the topographic survey and not for the GPR data acquisition per se. It is assumed that the electromagnetic waves do not interact with surface roughness components smaller than this threshold value. It is worth noting that this criterion is in close accordance with Rayleigh's criterion (see below). In this study, we operate in the frequency band 1-3 GHz. Consequently, min $\lambda = 0.1$ m and min $\Delta x = 0.01$ m. We used a 1 m long mechanical needle-like profiler consisting of a wood plate with an aluminum rod fixed at its basis. Upon this rod, there are 99 holes 0.01 m apart through which aluminum needles slide. Two poles and a spirit level are used to sustain the profiler horizontally. When the profiler is mounted, the needles are placed on the ground, and their upper tips delineate the profile of the soil situated below the plate. Then a picture of the profile is taken. Finally, digitization of the picture is performed in order to transform the profile into horizontal and vertical coordinates. An advantage of the needle-like profiler, compared to the meshboard profiler for instance, is that the soil profile is reproduced by the upper part of the needles. Then, the picture of the soil profile is well contrasted and can be taken at the same level, eliminating parallax errors. The main source of error affecting our mechanical measurements was the change in soil surface produced by the needles when they touch the sand, which was particularly crumbly in dry conditions.

[23] Figure 4 shows surface topography and the autocorrelation function measures along a profile. The mean

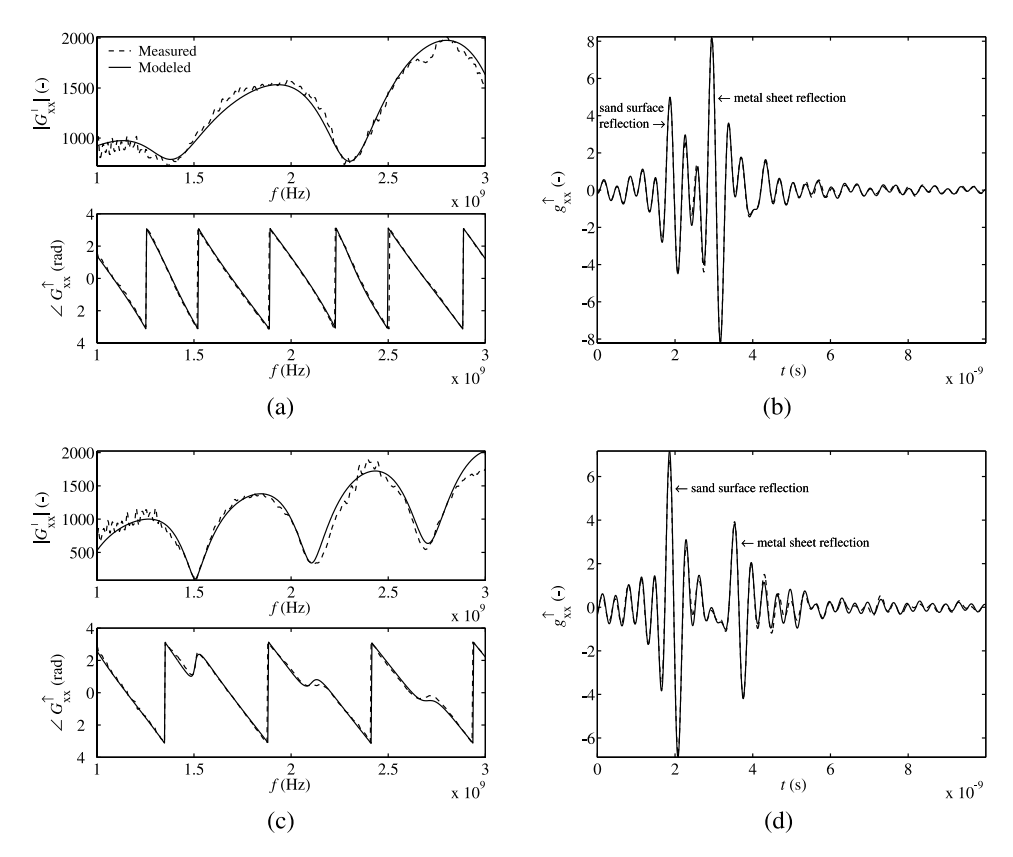


Figure 5. Measured and modeled Green's function for the (a, b) $\theta = 0.03$ and (c, d) $\theta = 0.15$ water contents, when the sand surface is smooth. Data are presented in both the frequency (Figures 5a and 5c) and time domains (Figures 5b and 5d).

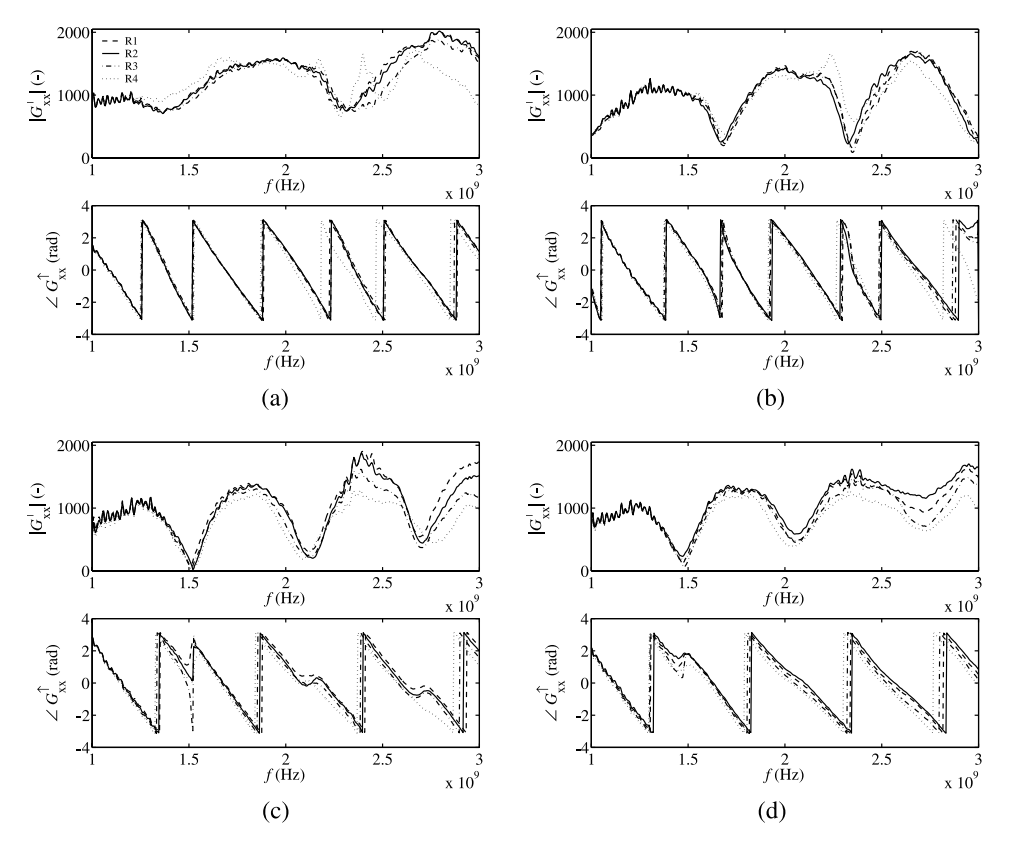


Figure 6. Effect of soil roughness (R₁, s = 0.00 and $h_{\text{max}} = 0$ cm; R₂, s = 0.27 and $h_{\text{max}} = 1.4$ cm; R₃, s = 0.47 and $h_{\text{max}} = 2.2$ cm; R₄, s = 0.72 and $h_{\text{max}} = 3.8$ cm) on the measured Green's function G_{xx}^{\uparrow} for water contents (a) $\theta = 0.03$, (b) $\theta = 0.12$, (c) $\theta = 0.15$, and (d) $\theta = 0.19$.

elevation of the surface has been subtracted from all height data. In this case, the autocorrelation function is identical to the autocovariance function, and the square root of the height variance is the standard deviation s around zero mean. In this example, we observe a correlation length of ~ 2.8 cm. In all roughness scenarios considered in this study, except for the smooth surface case, the size of the 3 dB antenna footprint was several times larger than the correlation length, which varied from about 2 to 5 cm. This is illustrated in Figure 4.

3. Results and Discussion

3.1. Effect of Surface Roughness on the GPR Signal

[24] Figure 5 shows, in both the frequency and time domains, the measured and modeled Green's functions pertaining to volumetric water contents $\theta = 0.03$ and $\theta = 0.15$ for the smooth sand scenario. The electromagnetic model shows remarkable agreement with the measurements. Thanks to the improved antenna transfer functions, this constitutes an improvement compared to the results presented by *Lambot et al.* [2004d] for a similar model configuration. In addition to the inherent VNA measurement errors, the remaining discrepancies observed may be attributed to the limited size of the metal sheet and sand box used (in the electromagnetic model they are assumed to be horizontally infinite), to the relatively small distance (23 cm) between the antenna and the sand surface which may be critical (the sand is not in the theoretical far field of the

antenna, whose upper limit is 51 cm at 3 GHz), and to the presence of ambiguous wave reflections from extraneous objects present in the laboratory.

[25] Figure 6 represents the measured Green's functions in the frequency domain for four different water contents $(\theta = 0.03 \text{ (6a)}, \theta = 0.12 \text{ (6b)}, \theta = 0.15 \text{ (6c)}, \text{ and } \theta = 0.19$ (6d)) and the four considered roughness levels. Roughness is quantified by the standard deviation s of the elevations and the average maximal amplitude h_{max} of the protuberances. The Green's function is weakly affected in the frequency range 1-1.5 GHz. Then, compared to the reference smooth surface scenario R₁, the discrepancy increases with both frequency and roughness amplitude. Specular reflection, which is the main reflection measured by the antenna, decreases with both surface roughness and frequency to the benefit of diffuse reflection, which is poorly measured by the antenna. For the two lower water contents $\theta = 0.03$ and $\theta = 0.12$, the effect is random. However, for water contents higher than 0.12, a more linear behavior may be observed, with the Green's functions decreasing with increasing surface roughness. In addition to the differences in surface topography, this may be explained by the fact that when the water content is low, the main part of the measured wave has propagated two times through the rough sand surface and sand layer (the metal sheet reflection being the most important, as illustrated in Figure 5), whereas when the water content is high, the main part of the measured wave has only reflected on the sand surface.

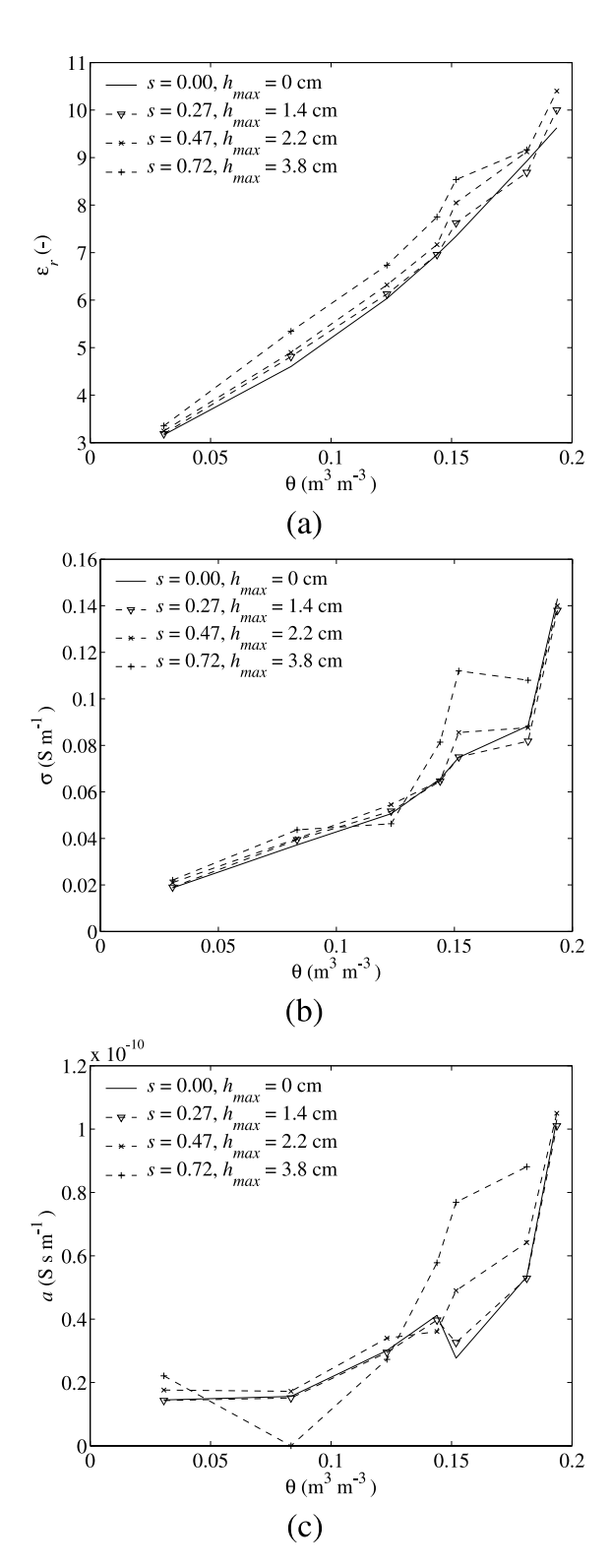


Figure 7. (a) Inversely derived relative dielectric permittivity ε_r , (b) average electric conductivity σ at 2 GHz, and (c) frequency dependence a (see equation (9)) of the electric conductivity of the sand layer as a function of its water content (θ) for the different surface roughness levels. Here s is the standard deviation characterizing surface roughness, and $h_{\rm max}$ represents the maximum average amplitude of roughness.

3.2. Effect of Surface Roughness on the Estimated Soil Electromagnetic Properties

[26] Figure 7 represents the inversely estimated soil electromagnetic properties for the 7×4 scenarios. Results are consistent and the error on the estimated parameters increases with roughness. The dielectric permittivity is generally overestimated. This may be explained by the existing negative correlation of this parameter with the thickness h of the sand layer (see Lambot et al. [2004c] for the same one-layer configuration). The electric conductivity and its frequency dependence are also overestimated when roughness is present. This originates from the model compensation accounting for the specular reflection energy, which is lost due to rough surface scattering (a high electric conductivity also has the effect of attenuating the wave energy in the layer and thus to decrease the measured field amplitude).

[27] From these results, it appears that the solution of the inverse problem is stable with respect to roughness modeling errors. In quite a continuous way, an increasing error on the estimated parameters is observed as a function of roughness. This consistence demonstrates the well posedness of the inverse problem dealt with and the stability properties of the inverse solution. For example, we can observe that if the ratio between the average wavelength and the maximal amplitude of the surface protuberances is 1/4, then the absolute error made on the GPR derived relative dielectric permittivity is about 1, and the corresponding absolute error on the estimation of the volumetric water content is about 0.02-0.04. It is worth noting that the reflecting metal sheet makes a significant contribution to the signal (see Figure 5), especially for low water contents, but would not be a component of more realistic data collection in the field. Nevertheless, we can observe on Figure 7 that when the contribution of the reflecting metal sheet decreases substantially, due to an increase in water content, the results are not affected and the effects of surface roughness remain comparable.

3.3. Roughness Criterion

[28] Defining a surface from an electromagnetic point of view as smooth or rough is obviously somewhat arbitrary and subjective. Nevertheless several criteria can be found in the literature to define a smooth surface. The most commonly used is Rayleigh's criterion [e.g., see *Boithias* 1987]. For a monostatic mode of operation (normal incidence), the critical height h_c of the surface protuberances is defined as $h_c = \lambda/8$, where λ is the wavelength. A surface is considered as rough if $h > h_c$. Ulaby et al. [1986] proposed the usage of the more stringent Fraunhofer criterion for better estimations above microwave frequencies (>1 GHz). At normal incidence, this criterion considers a surface as smooth if $h_c < \lambda/32$. This criterion results from the demand that the root-mean-square phase difference between two rays reflected at two different heights on the surface must be small enough in the far field in order to combine coherently, i.e., the rays are almost "in phase," as in the case of a perfectly smooth surface.

[29] Figure 8 represents the amplitude of the error between the modeled and measured Green's functions as a function of frequency and roughness. The shaded area delineates the 99% confidence interval threshold value

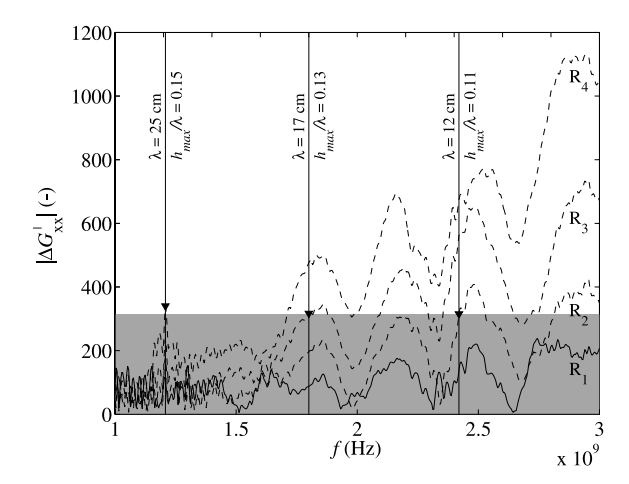


Figure 8. Amplitude of the averaged error between the modeled and measured Green's functions as a function of surface roughness. Here λ is the wavelength, and $h_{\rm max}$ is the maximal amplitude of the protuberances. The shaded area limits a threshold above which the deviation is outside the 99% confidence interval when compared to the smooth cases.

under which the error, assumed to be Gaussian distributed, is considered as normal. We computed this threshold value from the error pertaining to the smooth case (R_1). For R_2 , R_3 and R_4 , the frequency above which the threshold is overstepped is marked by a triangular symbol. We can observe that the ratio between the roughness amplitude h_{max} and the critical wavelength varies from 0.11 (1/9) to 0.15 (1/6.7), which is well in accordance with Rayleigh's criterion (1/8).

3.4. Practical Considerations

[30] In this paper, we considered only a 9 cm thick soil layer above a metal sheet. The results presented are directly applicable for similar model configurations under controlled conditions, as by Lambot et al. [2004a] for instance. However, in practical field applications, the metal sheet is absent, the soil layering is unknown, and the soil electromagnetic properties may vary laterally and in depth. As a result, more advanced or specific inverse modeling strategies are required to analyze the GPR data, for example, as by Lambot et al. [2004b, 2005b], and the effect of surface roughness on the inverse identification of the soil properties may be different. For instance, it is usual in natural conditions that the top 1 cm or so of the soil dries out rapidly, while higher moisture is retained below for longer periods. In this case, the effect of surface roughness may be reduced to a certain degree, due to the low contrast between the dielectric permittivity of that layer with air. This effect is clearly shown on Figure 6, where the Green's function decreases less in dryer conditions.

[31] Even if in this paper the reflecting metal sheet makes a significant contribution to the signal, we observe that the results are not affected when this contribution decreases substantially due to an increase in water content. In addition, we expect that the inverse solution will remain stable for different layer thicknesses. This is because different water contents to which the sand layer was subject lead to different propagation velocities, which emulate layers of different thicknesses.

[32] One of the most promising applications of the GPR approach and results presented in this paper is mapping of the surface soil moisture. In this case, we can focus only on the surface reflection and the model configuration is close to the one investigated here for the higher water contents, in which case the metal sheet is almost invisible.

4. Conclusions

[33] The outcome of this paper is twofold. First we show that determining the three antenna transfer functions in the model of $Lambot\ et\ al.$ [2004d], namely, H_i , H_i , and H_f , from only three model configurations leads inherently to large errors (sometimes tending to infinity) for some specific frequencies and therefore can lead also to significant errors on the inverse identification of the soil electromagnetic properties. To circumvent this issue, we propose to use additional model configurations, i.e., to overdetermine the system of equations. Experimental data based on six calibration configurations at different heights above a metal sheet significantly improved the determination of the antenna transfer functions.

[34] Then, we investigate the effect of soil surface roughness on the GPR signal and on the inverse identification of the soil electromagnetic properties. We demonstrated for a one-layered sand that the inverse solution is stable in relation to, or depends continuously on, the modeling errors caused by surface roughness. That means that small modeling errors will lead to small errors in the estimated parameters. For example, even at surface roughness of $\lambda/4$ the error of the water content measurement is only 2-4%. Larger ratios will lead to larger errors. Second, we show that the commonly used Rayleigh's criterion may be used to determine if a surface appears smooth to the radar, namely, the maximal height of the surface protuberances should be smaller than one eighth of the wavelength. This is an important result since this criterion can be used as a basis to evaluate the applicability of the technique under field conditions, e.g., for estimating soil water content and to accordingly determine the most appropriate operating radar frequency range. Practically, in cases where Rayleigh's criterion is satisfied, the method appears to be very promising for mapping the near surface water content in

[35] The next logical step is to implement existing soil surface scattering models including roughness, presently used for spaceborne radar data analysis, in the GPR electromagnetic model and to test if these models are able to reproduce the decreasing Green's function with respect to frequency, as we observed mainly for the higher water contents.

[36] Acknowledgments. This research was supported by a Marie Curie IntraEuropean Fellowship within the 6th European Community Framework Programme, the Université catholique de Louvain (Belgium), Royal Military Academy (Belgium), and Delft University of Technology (The Netherlands). We thank Mark P. Grasmueck and two anonymous reviewers for their constructive comments.

References

Balanis, C. A. (1997), Antenna Theory: Analysis and Design, John Wiley, Hoboken, N. J.

- Beckmann, P., and A. Spizzichino (1987), *The Scattering of Electromagnetic Waves From Rough Surfaces*, 2nd ed., Springer, New York.
- Boithias, L. (1987), Radio Wave Propagation, McGraw-Hill, New York. Chanzy, A., A. Tarussov, A. Judge, and F. Bonn (1996), Soil water content determination using digital ground penetrating radar, Soil Sci. Soc. Am. J., 60, 1318–1326.
- Chen, K., and A. Fung (1995), A comparison of backscattering models for rough surfaces, *IEEE Trans. Geosci. Remote Sens.*, 33, 195–200.
- Chen, M., and S. Bai (1990), Computer simulation of wave scattering from a dielectric random rough surface in two dimensions—Cylindrical case, *J. Electromagn. Waves Appl.*, 4, 919–1026.
- Davidson, M., T. Le Toan, F. Mattia, G. Satalino, T. Manninen, and M. Borgeaud (2000), On the characterization of agricultural soil roughness for radar remote sensing studies, *IEEE Trans. Geosci. Remote Sens.*, 38, 630–640.
- Davis, J. L., and A. P. Annan (2002), Ground penetrating radar to measure soil water content, in *Methods of Soil Analysis*, part 4, *Physical Methods*, edited by J. Dane and G. Topp, pp. 446–463, Soil Sci. Soc. of Am., Madison, Wis.
- Dierking, W. (1999), Quantitative roughness characterization of geological surfaces and implications for radar signature analysis, *IEEE Trans. Geosci. Remote Sens.*, 37, 2397–2412.
- Dogaru, T., and L. Carin (2001), Time-domain sensing of targets buried under a Gaussian, exponential, or fractal rough interface, *IEEE Trans. Geosci. Remote Sens.*, 39, 1807–1819.
- Du, S., and P. Rummel (1994), Reconnaissance studies of moisture in the subsurface with GPR, in *Proceedings of the Fifth International Conference on Ground Penetrating Radar*, edited by M. T. van Genuchten, F. J. Leij, and L. Wu, pp. 1241–1248, Waterloo Cent. for Groundwater Res., Univ. of Waterloo, Waterloo, Ont., Canada.
- El-Shenawee, M., and E. Miller (2004), Multiple-incidence and multifrequency for profile reconstruction of random rough surfaces using the 3-D electromagnetic fast multipole model, *IEEE Trans. Geosci. Remote Sens.*, 42, 2499–2510.
- Fung, A., Z. Li, and K. Chen (1992), Backscattering from a randomly rough dielectric surface, *IEEE Trans. Geosci. Remote Sens.*, 30, 356–369.
- Hallikainen, M., F. Ulaby, M. Dobson, M. El-Rayes, and L. Wu (1985), Microwave dielectric behavior of wet soil, part I: Empirical models and experimental observations, *IEEE Trans. Geosci. Remote Sens.*, 23, 25– 34.
- Hastings, F., J. Schneider, and S. Broschat (1995), A Monte-Carlo FDTD technique for rough surface scattering, *IEEE Trans. Antennas Propag.*, 43, 1183–1191.
- Heimovaara, T., E. de Winter, W. van Loon, and D. Esvald (1996), Frequency dependent dielectric permittivity from 0-1 GHz: Time domain reflectometry measurements compared with frequency domain network analyser measurements, *Water Resour. Res.*, 32, 3603–3610.
- Hipp, J. (1974), Soil electromagnetic parameters as functions of frequency, soil density, and soil moisture, *Proc. IEEE*, 62, 88-103.
- Huisman, J., C. Sperl, W. Bouten, and J. Verstraten (2001), Soil water content measurements at different scales: Accuracy of time domain reflectometry and ground penetrating radar, *J. Hydrol.*, 245, 48–58.
- Huisman, J., S. Hubbard, J. Redman, and A. Annan (2003), Measuring soil water content with ground penetrating radar: A review, *Vadose Zone J.*, 2, 476–491.
- Huyer, W., and A. Neumaier (1999), Global optimization by multilevel coordinate search. *J. Global Optim.*, 14, 331–355.
- Lagarias, J., J. Reeds, M. Wright, and P. Wright (1998), Convergence properties of the Nelder-Mead simplex method in low dimensions, SIAM J. Optim., 9, 112–147.
- Lambot, S., M. Javaux, F. Hupet, and M. Vanclooster (2002), A global multilevel coordinate search procedure for estimating the unsaturated soil hydraulic properties, *Water Resour. Res.*, 38(11), 1224, doi:10.1029/ 2001WR001224.
- Lambot, S., M. Antoine, I. van den Bosch, E. Slob, and M. Vanclooster (2004a), Electromagnetic inversion of GPR signals and subsequent hydrodynamic inversion to estimate effective vadose zone hydraulic properties, *Vadose Zone J.*, 3, 1072–1081.
- Lambot, S., J. Rhebergen, I. van den Bosch, E. Slob, and M. Vanclooster (2004b), Measuring the soil water content profile of a sandy soil with an off-ground monostatic ground penetrating radar, *Vadose Zone J.*, 3, 1063–1071.
- Lambot, S., E. Slob, I. van den Bosch, B. Stockbroeckx, B. Scheers, and M. Vanclooster (2004c), Estimating soil electric properties from mono-

- static ground-penetrating radar signal inversion in the frequency domain, *Water Resour. Res.*, 40, W04205, doi:10.1029/2003WR002095.
- Lambot, S., E. Slob, I. van den Bosch, B. Stockbroeckx, and M. Vanclooster (2004d), Modeling of ground-penetrating radar for accurate characterization of subsurface electric properties, *IEEE Trans. Geoscience Remote Sens.*, 42, 2555–2568.
- Lambot, S., I. van den Bosch, B. Stockbroeckx, P. Druyts, M. Vanclooster, and E. Slob (2005a), Frequency dependence of the soil electromagnetic properties derived from ground-penetrating radar signal inversion, Subsurface Sens. Technol. Appl., 6, 73–87.
- Lambot, S., L. Weihermüller, I. van den Bosch, M. Vanclooster, and E. C. Slob (2005b), Full-wave inversion of off-ground monostatic GPR signal focused on the surface reflection for identifying surface dielectric permittivity, in *Proceedings of the 3rd International Workshop on Advanced Ground Penetrating Radar*, edited by S. Lambot and A. Gorriti, pp. 113–118, Delft Univ. of Technol., Delft, Netherlands.
- Lampe, B., and K. Holliger (2003), Effects of fractal fluctuations in topographic relief, permittivity and conductivity on ground-penetrating radar antenna radiation, *Geophysics*, 68, 1934–1944.
- Mancini, M., R. Hoeben, and P. Troch (1999), Multifrequency radar observations of bare surface soil moisture content: A laboratory experiment, Water Resour. Res., 35, 1827–1838.
- Michalski, K., and J. Mosig (1997), Multilayered media Green's functions in integral equation formulations, *IEEE Trans. Antennas Propag.*, 45, 508-519.
- Michalski, K., and D. Zheng (1990), Electromagnetic scattering and radiation by subsurfaces of arbitrary shape in layered media: Parts I and II, IEEE Trans. Antennas Propag., 38, 335–352.
- O'Neill, K., R. Lussky, and K. Paulsen (1996), Scattering from a metallic object embedded near the randomly rough surface of a lossy dielectric, *IEEE Trans. Geosci. Remote Sens.*, 34, 367–376.
- Peterson, A. F., S. L. Ray, and R. Mittra (1998), Computational Methods for Electromagnetics, Oxford Univ. Press, New York.
- Sai, B., and L. Ligthart (2004), GPR phase-based techniques for profiling rough surfaces and detecting small, low-contrast landmines under flat ground, *IEEE Trans. Geosci. Remote Sens.*, 42, 318–326.
- Slob, E., and J. Fokkema (2002), Coupling effects of two electric dipoles on an interface, *Radio Sci.*, 37(5), 1073, doi:10.1029/2001RS002529.
- Tai, C.-T. (1994), Dyadic Green Function in Electromagnetic Theory, IEEE Press, Piscataway, N. J.
- Ulaby, F., M. Moore, and A. Fung (1986), Microwave Remote Sensing: Active and Passive, vol. III, From Theory to Applications, Artech House, Norwood, Mass.
- van Overmeeren, R., S. Sariowan, and J. Gehrels (1997), Ground penetrating radar for determining volumetric soil water content: Results of comparative measurements at two test sites, *J. Hydrol.*, 197, 316–338.
- Warnick, K., and W. Chew (2001), Numerical simulation methods for rough surface scattering, *Waves Random Media*, 11, R1–R30.
- Weiler, K., T. Steenhuis, J. Boll, and K.-J. Kung (1998), Comparison of ground penetrating radar and time domain reflectometry as soil water sensors, Soil Sci. Soc. Am. J., 62, 1237–1239.
- West, L., K. Handley, Y. Huang, and M. Pokar (2003), Radar frequency dielectric dispersion in sandstone: Implications for determination of moisture and clay content, *Water Resour. Res.*, 39(2), 1026, doi:10.1029/2001WR000923.
- Yarovoy, A., C. Vazouras, J. Fikioris, and L. Lighart (2004), Numerical simulations of the scattered field near a statistically rough air-ground interface, *IEEE Trans. Antennas Propag.*, 52, 780–789.
- Zhang, G., L. Tsang, and K. Pak (1997), Studies of the correlation function of scattering by random rough surfaces with and without a buried object, *IEEE Trans. Geosci. Remote Sens.*, 35, 444–453.
- M. Antoine and M. Vanclooster, Department of Environmental Sciences and Land Use Planning, Université catholique de Louvain, Croix du Sud 2 Box 2, B-1348 Louvain-la-Neuve, Belgium.
- S. Lambot, Agrosphere (ICG-IV), Institute of Chemistry and Dynamics of the Geosphere, Forschungszentrum Jülich GmbH, D-52425 Jülich, Germany. (s.lambot@f2-juelich.de)
- E. C. Slob, Department of Geotechnology, Delft University of Technology, Mijnbouwstraat 120, 2628 RX Delft, Netherlands.